

UNC13B regulates the sensitivity of Wilms' tumor cells to doxorubicin by modulating lysosomes

XI CHEN¹, YINGYING BAO¹, GE SUN¹, XIAOBO WANG² and JIAJUN ZHU^{1,3}

¹Department of Neonatology, Women's Hospital, School of Medicine, Zhejiang University, Hangzhou, Zhejiang 310006, P.R. China;

²Department of Hematology, The Seventh Affiliated Hospital, Sun Yat-Sen University, Shenzhen, Guangdong 518107, P.R. China;

³Zhejiang Provincial Clinical Research Center for Child Health, Hangzhou, Zhejiang 310006, P.R. China

Received February 15, 2024; Accepted June 14, 2024

DOI: 10.3892/ol.2024.14579

Abstract. Wilms' tumor is a malignant neoplasm where current medical advancements have significantly improved survival rates; however, challenges persist such as the resistance of the tumor to chemotherapy drugs like doxorubicin. This necessitates higher dosages, leading to decreased sensitivity. However, using high doses of doxorubicin can have late effects on the heart. Unc-13 homolog B (UNC13B) may be involved in the drug resistance in several tumors, yet its role in modulating drug sensitivity in Wilms' tumor remains unexplored. UNC13B levels were quantified using reverse transcription-qPCR and Western blotting. The half-maximal inhibitory concentration for doxorubicin, vincristine, and actinomycin-D was determined using CCK-8 assays. Cell cycle and apoptosis were analyzed using flow cytometry, and lysosomal changes were observed using Lyso-Tracker staining. The present study initially evaluated UNC13B expression levels in the Wilms' tumor 17.94 cell line. Additionally, through short hairpin RNA-mediated knockdown, changes in doxorubicin sensitivity in 17.94 Wilms' tumor cells were assessed. Concurrently, preliminary investigations into the role of UNC13B in regulating lysosomes was performed, revealing a significant positive association between UNC13B levels and lysosome formation in the 17.94 cell line. Lysosomes likely serve a role in the sensitivity of Wilms' tumor cell lines to drugs. Elevated UNC13B expression was observed in the 17.94 Wilms' tumor cell line compared to normal kidney cells. UNC13B knockdown also resulted in increased apoptosis levels upon doxorubicin treatment. Immunofluorescence

revealed UNC13B localization within cellular vesicles, and its knockdown significantly decreased lysosome levels. Overall, the findings of the present study demonstrate that UNC13B regulates the sensitivity of the Wilms' tumor 17.94 cell line to doxorubicin by modulating lysosome formation within cells. The results suggest that UNC13B is likely an enriched target involved in lysosomal regulation in certain tumors, offering a new approach for optimizing chemotherapy in Wilms' tumor and other cancers with high UNC13B expression.

Introduction

Wilms' tumor is the second most common intra-abdominal cancer in childhood and the fifth most frequent pediatric malignancy, constituting ~6% of all childhood cancers and >95% of all renal tumors in the pediatric age group in Europe (1,2). Furthermore, Wilms' tumor, also known as nephroblastoma, is among the most common primary malignant tumors of the kidneys in children, typically originating from embryonic kidney tissues. Despite significant advancements in treatment, managing advanced, anaplastic, or recurrent cases remains challenging due to the lack of curative therapies and significant long-term effects (3,4), particularly in chemotherapy and tumor cell growth regulation. Currently, the treatment of Wilms' tumor globally falls into two categories: The Children's Oncology Group, primarily in North America, recommends direct surgical intervention followed by further treatment based on postoperative pathology and staging (5); whilst the International Society of Paediatric Oncology Renal Tumour Study Group, predominantly in Europe, advocates for preoperative chemotherapy, followed by surgical excision after tumor reduction, tailored according to varying risk levels (6).

Chemotherapeutic drugs used in the treatment of Wilms' tumor primarily act by disrupting cell DNA synthesis and the cell cycle. Commonly used drugs include vincristine, actinomycin-d, cyclophosphamide and doxorubicin (7-9); however, during the administration of these drugs, factors such as patient age and dosage can lead to late effects such as bowel obstruction and heart problems (10). Therefore, enhancing tumor cell sensitivity to chemotherapeutic drugs and reducing dosages are crucial in Wilms' tumor chemotherapy.

In our previous study, the regulation of unc-13 homolog B (UNC13B) in drug sensitivity was assessed in chronic

Correspondence to: Dr Jiajun Zhu, Department of Neonatology, Women's Hospital, School of Medicine, Zhejiang University, 1 Xueshi Road, Hangzhou, Zhejiang 310006, P.R. China
E-mail: jiajunzhu@zju.edu.cn

Dr Xiaobo Wang, Department of Hematology, The Seventh Affiliated Hospital, Sun Yat-Sen University, 628 Zhenyuan Road, Guangming, Shenzhen, Guangdong 518107, P.R. China
E-mail: wangxiaobo@sysush.com

Key words: unc-13 homolog B, Wilms' tumor, doxorubicin, lysosome

lymphoid leukemia. UNC13B was demonstrated to regulate tumor cell resistance to arsenic trioxide (11). These findings suggest a potential involvement of UNC13B in chemotherapeutic drug resistance in tumor cells. The development of chemotherapeutic drug resistance involves both external and internal factors, including tumor heterogeneity, the tumor microenvironment and the inactivation of anticancer drugs (12). Current research about UNC13B mainly focuses on brain and neural studies, where it serves a crucial role in synaptic vesicle initiation and fusion (13,14), potentially influencing neuronal excitability (15). As a regulator of the cell vesicular system, whether UNC13B mediates mechanisms of chemotherapeutic drug resistance in tumor cells through vesicle regulation remains unclear. Thus, the present study aims to assess the role of UNC13B in regulating drug sensitivity and resistance to doxorubicin in Wilms' tumor cell lines.

Materials and methods

Cell lines and drug treatment. The human Wilms' tumor 17.94 cell line was purchased from the Leibniz Institute, Deutsche Sammlung von Mikroorganismen und Zellkulturen-German Collection of Microorganisms and Cell Cultures GmbH (cat. no. ACC 741) and cultured in high-glucose DMEM supplemented with 20% FBS (HyClone; cat. no. SH30088.03) and 1% penicillin/streptomycin at 37°C in 5% CO₂. The human Ewing sarcoma SK-NEP-1 (cat. no. HTB-48) and human rhabdoid tumor G401 (cat. no. CRL-1441) cell lines were purchased from the American Type Culture Collection (ATCC) and maintained in McCoy's 5A modified medium containing 15% FBS (HyClone, SH30088.03). The human HK-2 normal kidney-derived proximal tubular cell line was purchased from Procell Life Science & Technology Co., Ltd. (cat. no. CL-0109) and cultured in MEM supplemented with 10% FBS (HyClone Laboratories, SH30088.03) and 1% penicillin/streptomycin at 37°C in 5% CO₂. The human kidney rhabdoid tumor WT-CLS1 cell line was purchased from CLS Cell Lines Services GmbH (cat. no. 300379) and cultured in IMDM supplemented with 10% FBS (HyClone Laboratories, SH30088.03) and 1% penicillin/streptomycin at 37°C in 5% CO₂. Authentication of the cell lines used in the present study was performed using Short Tandem Repeat (STR) profiling, provided by Pricella Biotechnology Co., Ltd (Elabscience Bionovation Inc.). This method involved analyzing specific STR loci to confirm the identity of the cell lines. Comparison of the STR profile of the samples in the present study against known reference profiles (source: ATCC) demonstrated a 100% match, ensuring the authenticity of the cell lines used in the experiments.

The determination of the half-maximal inhibitory concentration (IC₅₀) was performed as follows: Passaged cells were counted and seeded at a density of 3,000 cells per well in a 96-well plate. Following overnight incubation at 37°C, 0.1–5 µM doxorubicin (cat. no. E2516; Selleck Chemicals), 0–500 nM vincristine sulfate (cat. no. S1241; Selleck Chemicals) or 0.1–5 nM actinomycin-D (cat. no. S8964; Selleck Chemicals) in DMSO were added, whilst the negative control group received an equal volume of DMSO. Each group was set up with 6 replicates. After incubation for 48 h at 37°C in 5% CO₂, 10 µl Cell Counting Kit-8 (CCK-8) reagent

(cat. no. C0038; Beyotime Institute of Biotechnology) was added per well, followed by an additional 4-h incubation in the culture chamber. The optical density at 450 nm was measured using a microplate reader. IC₅₀ was calculated using GraphPad Prism 9.0 software (Dotmatics). After entering data into GraphPad Prism, a nonlinear regression (curve fit) analysis was used. The '(Inhibitor) vs. normalized response-Variable slope' model was chosen. A curve was generated to fit the data, and the IC₅₀ value was displayed. This value represented the concentration of the compound at which the response was half of the maximum effect observed.

Short hairpin (sh)RNA construction and transfection. The construction of shRNA followed a previously described method (11). Based on the nucleotide sequence of UNC13B in the GenBank database (ncbi.nlm.nih.gov/nuccore/NM_001371189.2, ID no. NM_001371189.2), 17.94 cells were transfected with UNC13B shRNA (shUNC13B) using a lentivirus vector. The second-generation lentiviral vector system was used to construct shRNA lentivirus. The plasmid backbone and negative controls are as follows: lentiCRISPR v2 (cat. no. 52961; Addgene, Inc.), pCMV-pVSV-G (cat. no. 8454; Addgene, Inc.), and psPAX2 (cat. no. 12260; Addgene, Inc.). The negative controls are scramble sequences synthesized by igebio biotech Co., Ltd. UNC13B shRNA lentiviral vector using lentiCRISPR v2. (cat. no. 52961; Addgene, Inc.) was constructed. The sequence of the sense strand of shUNC13B was 5'-CGAGTCCTATGAGTTGCAGAT-3' and the antisense strand was 5'-ATCTGCAACTCATAGGACTCG-3'. Cells were also transfected with non-target shRNA as a negative control (shCtrl; scramble). The sequence of the sense strand was 5'-CCTAAGGTAAAGTCGCCCTCGC-3' and the antisense strand was 5'-GCGAGGGCGACTTAACCTTAGG-3', connected by a 'TCGA' loop, with an additional 5 thymine (T) at the end. Scrambled shRNA is designed so that it does not target any specific mRNA for degradation (16). All shRNAs were synthesized by igebio biotech Co., Ltd. shRNA was inserted into the lentiCRISPR v2 plasmid using AgeI and EcoRI restriction enzyme sites. The plasmid was then transformed into DH5α cells (Beyotime, D1031S) for amplification. After amplification, the plasmid was purified using the Endo-Free Plasmid Midi Kit (Omega Bio-Tek, D6915). The purified plasmid was verified by sequencing to ensure the correct insert.

Lipofectamine 3,000 (cat. no. L3000015; Invitrogen™; Thermo Fisher Scientific, Inc.) was used to transfect these shRNAs into 293T cells (cat no. CL-0005; Procell Life Science & Technology Co., Ltd.), cultured in DMEM supplemented with 10% FBS (HyClone Laboratories, SH30088.03) and 1% penicillin/streptomycin at 37°C in 5% CO₂ for 48 h, along with the packaging plasmids pCMV-pVSV-G (cat. no. 8454; Addgene, Inc.) and psPAX2 (cat. no. 12260; Addgene, Inc.). Transfect with a ratio of 10 µg of psPAX2 plasmid, 10 µg of lentiCRISPR v2 plasmid containing the inserted shRNA, and 5 µg of pCMV-VSV-G plasmid into a 10 cm dish of 293T cells at approximately 80% confluence. The transfection duration was 12 h at 37°C, after which the medium was replaced. Lentiviral particles were collected and used to infect 17.94 cells at a multiplicity of infection (MOI) of 10. The duration of transduction into 17.94 cells is

12 h. Gene expression and transcription levels were identified 24 h after transduction using qPCR and western blot methods. Subsequent experiments were conducted 24–48 h after transduction. To normalize the transfection efficiency, green fluorescent protein (GFP) cDNA was inserted into an empty lentiCRISPR v2 to construct a GFP-lentiviral vector. A transfection experiment was performed on 17.94 cells using GFP-lentivirus. A total of 24 h after transfection, the cells were analyzed using a fluorescence microscope.

Overexpression vector and knockout vector construction and transfection. The full-length UNC13B sequence was synthesized by General Biosystems, Inc. according to the GenBank database (ncbi.nlm.nih.gov/nuccore/NM_001371189.2/, ID no. NM_001371189.2) and inserted into the pcDNA3.1 vector using *Bam*HI and *Hind*III restriction enzyme sites. The plasmid is transformed into DH5 α (Beyotime, D1031S) for amplification. Plasmid is then purified using Endo-Free Plasmid Midi Kit (Omega Bio-Tek, D6915). The purified plasmid is verified by restriction enzyme digestion and sequencing to ensure the correct insert.

For overexpression experiments, Transfection was carried out using Lipofectamine™ 3,000 Transfection Reagent (cat. no. L3000015; Invitrogen™; Thermo Fisher Scientific, Inc.). 1 μ g of plasmid was used per well in a 12-well plate with a cell density of over 80%. The transfection duration was 12 h at 37°C, after which the medium was replaced. Post-transfection, overexpression levels were assessed after 48 h using western blot for subsequent experiments. An empty vector pcDNA3.1 was used as the negative control.

The second-generation lentiviral vector system was used to construct sgRNA lentivirus. The lentiCRISPR V2 plasmid (cat. no. 52961; Addgene, Inc.) was used. Two single guide (sg)RNAs targeting UNC13B, hUNC13B-KO-1: 5'-TGATCA GCCTTCCTGGGAACAGG-3' and hUNC13B-KO-2: 5'-TCT TCACATTCTGTACTTTCAGG-3', were inserted, respectively, and two plasmids were developed, each containing a different sgRNA. All sgRNAs were synthesized by igebio biotech Co., Ltd. Lipofectamine 3000 was used to co-transfect these sgRNAs into 293T cells (cat no. CL-0005; Procell Life Science & Technology Co., Ltd.), cultured in DMEM supplemented with 10% FBS and 1% penicillin/streptomycin at 37 °C in 5% CO₂ for 48 h, along with the packaging plasmids pCMV-pVSV-G (cat. no. 8454; Addgene, Inc.) and psPAX2 (cat. no. 12260; Addgene, Inc.). Cells were transfected with a ratio of 10 μ g of psPAX2 plasmid, 10 μ g of lentiCRISPR v2 plasmid containing the inserted shRNA, and 5 μ g of pCMV-VSV-G plasmid into a 10 cm dish of 293T cells at approximately 80% confluence. A total of two cas9 plasmids targeting UNC13B were generated. Both prepared lentiviruses were co-transduced into 17.94 cells at a MOI of 10. The duration of transduction was 12 h, after which the lentivirus is removed. At 24 h post-transduction, cells were diluted using a limited dilution method into a 96-well plate and cultured for 14 days at 37 °C in 5% CO₂ to establish single-cell clones of UNC13B-KO using puromycin (Beyotime, ST551) at a selection concentration of 4 μ g/ml and a maintenance concentration of 0.8 μ g/ml. We used PCR and sequencing methods, performed by GENEWIZ Biotechnology Co., Ltd., to identify the amplified single-cell

clones, confirming that the target locus had been successfully edited. Reverse transcription (RT)-quantitative (q)PCR and western blotting were used to assess the transcription and expression levels of UNC13B.

RT-qPCR. RT-qPCR for UNC13B was performed as previously described (11). Briefly, RNA extraction from samples was performed using TRIzol™ (cat. no. 15596018CN; Invitrogen; Thermo Fisher Scientific, Inc.), and the concentration and purity of the extracted RNA were measured using a NanoDrop™ 2000 (Thermo Fisher Scientific, Inc.) to ensure its suitability for subsequent experimental procedures. The RNA was reverse transcribed into cDNA using a cDNA synthesis kit (EasyScript® First-Strand cDNA Synthesis SuperMix, TransGen Biotech, AE301-03) according to the manufacturer's instructions. The sequences for UNC13B were as follows: UNC13B forward, 5'-CCAGCTACACAACTCACTGAGG-3' and UNC13B reverse, 5'-CTGGTCAGCAAATCCACTGTG G-3'. The sequences for the reference gene 18SN5 were as follows: 18SN5 forward, 5'-ACCCGTTGAACCCCATTCGTG A-3' and 18SN5 reverse, 5'-GCCTCACTAAACCATCCAATC GG-3'. Hieff qPCR SYBR Green Master Mix (No Rox) from YEASEN (catalog number 11201ES08) was used with the Bio-Rad CFX96™ system. The thermocycling conditions for the qPCR assay were as follows: initial denaturation at 95°C for 5 min; 40 cycles of 95°C for 10 sec and 60°C for 30 sec; the melt curve stage followed the instrument's default settings. The following steps were used to validate the results of the RT-qPCR assays: The efficiency of the qPCR reaction was determined by running a standard curve with serial dilutions of a known template; the efficiency of the UNC13B primers was ~95%. After amplification, a melting curve analysis revealed a single, sharp peak, indicating the specificity of the PCR amplification. In each experiment, three technical replicates were performed to assess the consistency of the results. The 18SN5 gene was used as the reference gene, and the 2^{- $\Delta\Delta$ C_q} method (17) was used for quantification.

Western blot. 17.94, SK-NEP-1, G401, WT-CLS1, and HK-2 cells were lysed using RIPA buffer (Beyotime, P0013B), and protein concentration was measured using a BCA protein determination kit (Abcam). For SDS-PAGE, 20 μ g of protein was loaded/lane. The separating gel used was 12%. After electrophoresis, proteins were electrotransferred to a polyvinylidene fluoride membrane, which was blocked with 5% BSA (cat. no. V900933; Vetec™; Sigma-Aldrich; Merck KGaA)/TBST (0.1% Tween 20) at room temperature for 2 h. Rabbit polyclonal UNC13B (1:1,000; cat. no. NBP2-93337; Novus Biologicals, Ltd.) and mouse monoclonal lysosomal-associated membrane protein 1 (LAMP1; 1:1,000; cat. no. sc-20011; Santa Cruz Biotechnology, Inc.) primary antibodies were added at the appropriate dilution and incubated at 4°C overnight. Corresponding secondary antibodies, HRP-conjugated goat anti-mouse (1:10,000; cat. no. 7076; Cell Signaling Technology, Inc.) or anti-rabbit (1:10,000; cat. no. 7074; Cell Signaling Technology, Inc.), were added and incubated at room temperature for 2 h. HRP-labeled GAPDH (1:5,000; cat. no. 3683; Cell Signaling Technology, Inc.) was used as an internal reference. Membranes were incubated for 3 min in Supersignal West Pico Plus Chemiluminescent

Substrate (Thermo Scientific, 34580) and exposed using the iBright FL1000 Imaging System (Thermo Fisher Scientific Inc.), and iBright Analysis Software (desktop version 5.1.0; Thermo Fisher Scientific Inc.) was used for semi-quantification.

Flow cytometry analysis. For cell cycle analysis, 17.94 cells were digested with trypsin, and the trypsin digestion was terminated using complete culture medium. The cells were washed once with pre-cooled serum-free medium and fixed with pre-cooled 75% ethanol overnight. Following a PBS wash and cell precipitation, the cells were stained with PI staining solution (cat. no. 40710ES03; Shanghai Yeasen Biotechnology Co., Ltd.) at 37°C for 30 min. Data collection was performed using a CytoFLEX LX Flow Cytometer (Beckman Coulter, Inc.), with 40,000 events collected for each sample. FlowJo 10.8.1 (Becton, Dickinson and Company) was used for data analysis.

For apoptosis analysis, an Annexin V-FITC/PI kit (cat. no. 40302ES60; Shanghai Yeasen Biotechnology Co., Ltd.) was used according to the manufacturer's instructions. Cells were digested with trypsin (without EDTA) and centrifuged at 300 x g and 4°C for 5 min. Cells were washed twice with pre-chilled PBS, each time centrifuging at 300 x g and 4°C for 5 min. Cells were collected, and 5x10⁵ cells were resuspended in 100 µl of 1X Binding Buffer. A total of 5 µl Annexin V-FITC and 10 µl PI Staining Solution were then added, and cells were incubated in the dark at room temperature for 10-15 min. Subsequently, 400 µl of 1X Binding Buffer was added and kept on ice. Samples were analyzed within 1 h using flow cytometry. Data collection was performed using a CytoFLEX LX Flow Cytometer, with 40,000 events collected for each sample. FlowJo 10.8.1 was used for data analysis.

Indirect immunofluorescence and lysosome staining. Indirect immunofluorescence was used to detect the localization of UNC13B in 17.94 cells. Initially, cell slides were prepared and fixed with 100% methanol at -20°C for 10 min. After three PBS washes, a blocking solution of 3% BSA (Sigma-Aldrich; Merck KGaA; cat. no. V900933) + 0.3% Triton™ X-100 in PBS was added at room temperature for 1 h. The blocking solution was removed, and the slides were incubated with rabbit UNC13B primary antibodies (1:200; cat. no. NBP2-93337; Novus Biologicals, Ltd.) at 4°C overnight. Following PBS washes (3 times for 5 min each), the slides were incubated with Goat Anti-Rabbit IgG H&L (Alexa Fluor® 488) secondary antibodies (1:2,000; cat. no. ab150077; Abcam) at room temperature for 1 h. The slides were then sealed with a mounting medium containing DAPI (cat. no. P0131; Beyotime Institute of Biotechnology) and images were captured using a confocal microscope.

Staining of cells with Lyso-Tracker Red (cat. no. L8010; Beijing Solarbio Science & Technology Co., Ltd.) was performed by preparing a final concentration of 50 nM Lyso-Tracker Red working solution. The cell culture medium was removed, and cells were incubated with pre-warmed Lyso-Tracker Red staining working solution at 37°C for 2 h. Following the incubation, the Lyso-Tracker Red staining solution was removed, and 2 µM Hoechst 33342 was added. The cells were then incubated at 37°C for an additional 30 min before replacing the medium with fresh cell culture medium.

Observations were performed using a confocal microscope, with an excitation wavelength of 577 nm and an emission wavelength of 590 nm during detection. The mean fluorescence intensity was calculated using ImageJ software (version 1.53q; National Institutes of Health).

Data analysis. For *in vitro* experiments, each experiment was independently repeated ≥3 times. Error bars indicate standard deviation. The unpaired Student's t-test was used for comparisons between two groups, whilst one-way ANOVA was used for multiple comparisons. Dunnett's test was used for post hoc analysis when all pairwise comparisons involved one specific group being compared with all other groups in the dataset. Tukey's test was used for post hoc analysis when comparing all possible pairs of mean. P<0.05 was considered to indicate a statistically significant difference. GraphPad 9.0 (Dotmatics) was used for statistical analysis and image generation.

Results

Elevated expression of UNC13B in Wilms' tumor cell line. Using commercially available 17.94 Wilms' tumor cell line (18), alongside other renal tumor cell lines, an Ewing sarcoma (SK-NEP-1) (19), a rhabdoid tumor (G-401) (20), a kidney rhabdoid tumor (WT-CLS1) and human normal renal cell lines (HK-2), an analysis of UNC13B transcription and expression levels was performed. The results revealed a significant increase in both the mRNA and protein expression levels of UNC13B in the 17.94 cell line compared with that in the HK-2 cell line (Fig. 1A and B). The UNC13B expression level in 17.94 cells was also notably higher compared with that in the other cell lines. Additionally, there was a clear positive association between mRNA and protein expression levels (Fig. 1A and B). Before shRNA knockdown experiment, we inserted GFP cDNA into an empty lentiCRISPR v2 vector to construct a GFP-lentiviral vector for verifying transfection efficiency. The GFP-lentivirus was transfected into 17.94 cells. After 24 h, fluorescence microscopy analysis showed that over 95% of the cells expressed GFP, indicating a transfection efficiency of over 95%. In shRNA knockdown experiments performed in 17.94 cells, a significant reduction in UNC13B mRNA levels was observed 48 h post-infection under knockdown condition compared with controls, with a multiplicity of infection (MOI) of 5 (Fig. 1C). Consequently, an MOI of 5 was selected for protein level validation post-knockdown, revealing a significant decrease in UNC13B expression levels compared with controls (Fig. 1D and E). Moreover, assessing the proliferation levels of knockdown cells revealed a significant reduction in cell proliferation following the reduction of UNC13B levels (Fig. 1F) compared with controls, which is consistent with findings from our previous study on UNC13B knockdown in other tumor cells (11).

UNC13B modulates Wilms' tumor cell sensitivity to doxorubicin, independent of the cell cycle. Building upon findings from our previous study (11), which indicated the involvement of UNC13B in tumor cell resistance to chemotherapy, the present study further assessed whether UNC13B is associated with drug resistance and sensitivity in Wilms' tumor cells. In clinical treatment for Wilms' tumor, chemotherapy

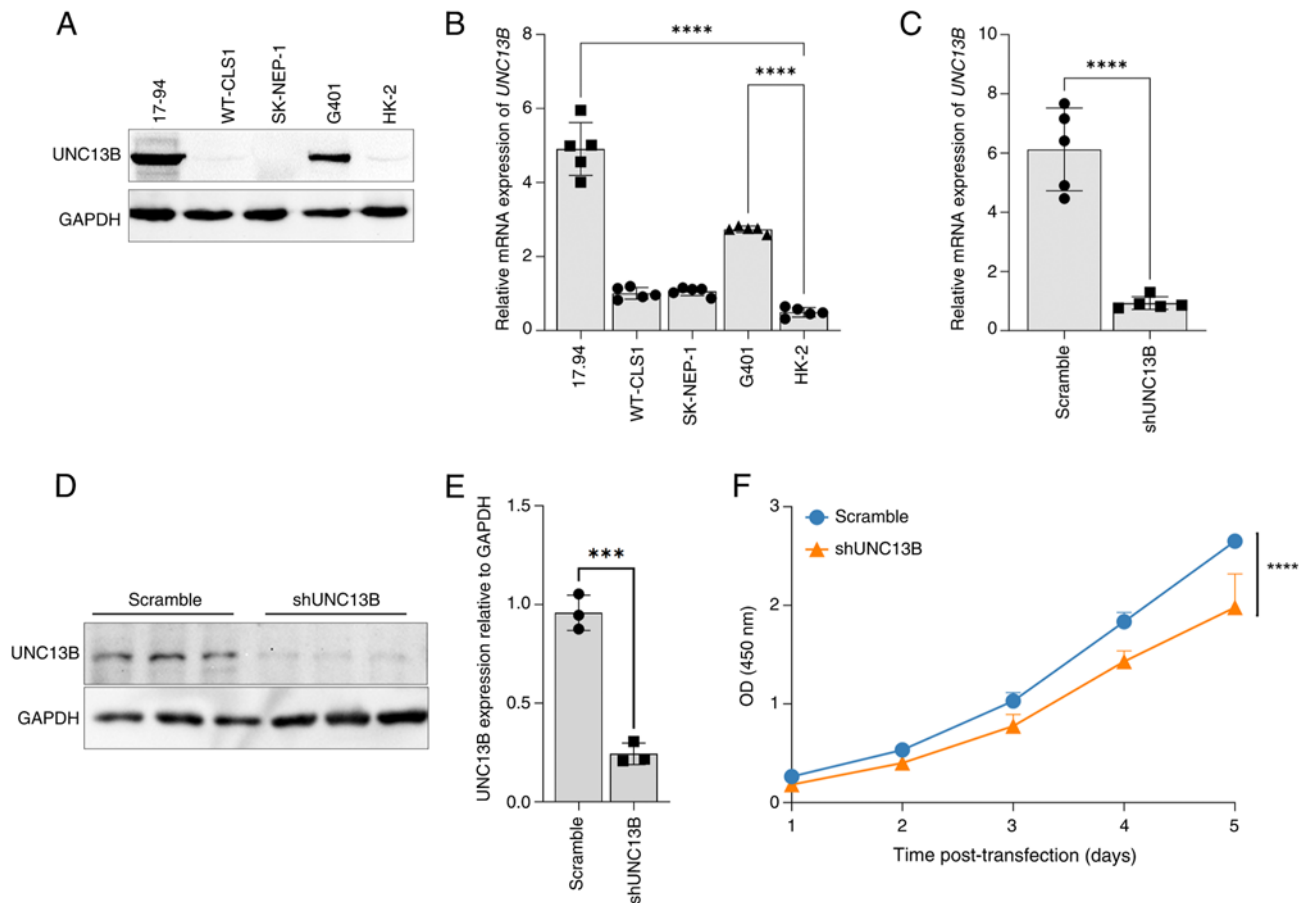


Figure 1. Elevated expression of UNC13B in Wilms' tumor cell lines. (A) Western blot analysis of UNC13B expression in WT-CLS1, 17.94, G401, SK-NEP-1 and HK-2 cells. Each lane was loaded with 20 μ g protein and GAPDH was used as a reference. (B) Analysis of UNC13B transcription levels in different cell lines; n=5. (C) Changes in UNC13B transcription levels 48 h post-shRNA-mediated UNC13B knockdown in 17.94 cells compared with the scramble control; n=5. (D) UNC13B expression changes 48 h post-shRNA-mediated knockdown in 17.94 cells and (E) statistical analysis of the expression level changes. Each experiment was repeated 3 times, with GAPDH used as a reference. (F) Assessment of cell proliferation post-knockdown using a Cell Counting Kit-8 assay, measuring OD450 values at different time points; n=3. Cells were also transfected with non-target scrambled shRNA as a control. ***P<0.001; ****P<0.0001. UNC13B, unc-13 homolog B; sh, short hairpin; OD, optical density.

drugs such as vincristine, doxorubicin and actinomycin-D are primarily used for preoperative treatment (21). Therefore, the altered sensitivity of UNC13B knockdown 17.94 cells to these drugs was analyzed. The results demonstrated that UNC13B knockdown notably increased the sensitivity of 17.94 cells to doxorubicin and actinomycin-D, although the IC₅₀ value for vincristine was lower in the UNC13B knockdown group (88.45 ± 12.16 vs. 59.06 ± 10.80 nM; Fig. 2A) compared to the scramble group, this difference was not statistically significant. Significantly lowering the IC₅₀ values for actinomycin-D (1.544 ± 0.09 vs. 1.005 ± 0.07 nM; Fig. 2B) and doxorubicin (1882 ± 124.3 vs. 697.2 ± 46.29 nM; Fig. 2C) compared to the scramble group. The changes in sensitivity to the aforementioned drugs were also tested in G401 cells after UNC13B knockdown. Following UNC13B knockdown, there was a significant decrease in the IC₅₀ for all three drugs: Vincristine (77.74 ± 6.82 vs. 33.17 ± 2.83 nM; Fig. 2D), actinomycin-D (1.524 ± 0.085 vs. 1.17 ± 0.056 nM; Fig. 2E) and doxorubicin ($1,018 \pm 65.23$ vs. 239.0 ± 30.14 nM; Fig. 2F) compare to the scramble group. This demonstrates that reducing UNC13B levels enhances the sensitivity of G401 cells to these drugs. Subsequently, the cell cycle changes upon doxorubicin treatment were evaluated to elucidate the role of UNC13B in

drug sensitivity and resistance. The results demonstrated that UNC13B had no notable impact on cell cycle alterations (Fig. 2G and H), suggesting the involvement of other mechanisms in UNC13B-mediated drug resistance in Wilms' tumor cells. Furthermore, apoptosis in 17.94 cells following UNC13B knockdown was analyzed. The results indicated that knockdown of UNC13B significantly increased apoptosis levels at 0.5 μ M doxorubicin (Fig. 2I and J) compared to the scramble group; however, at 2 μ M doxorubicin, the increase in apoptosis levels was significant but less pronounced. This suggests that UNC13B may negatively regulate the drug sensitivity of 17.94 cells to doxorubicin-induced apoptosis.

Involvement of UNC13B in Wilms' tumor lysosome formation. A previous report suggested an association between doxorubicin drug sensitivity and lysosomes (22). Additionally, several studies have highlighted the notable role of UNC13B in regulating synaptic vesicles (23,24). Hence, we hypothesized that UNC13B may modulate drug sensitivity by participating in vesicle regulation within cells and localization of UNC13B within the cellular vesicles was detected using an indirect immunofluorescence method. The results demonstrated the presence of UNC13B within the cellular vesicles (Fig. 3A),

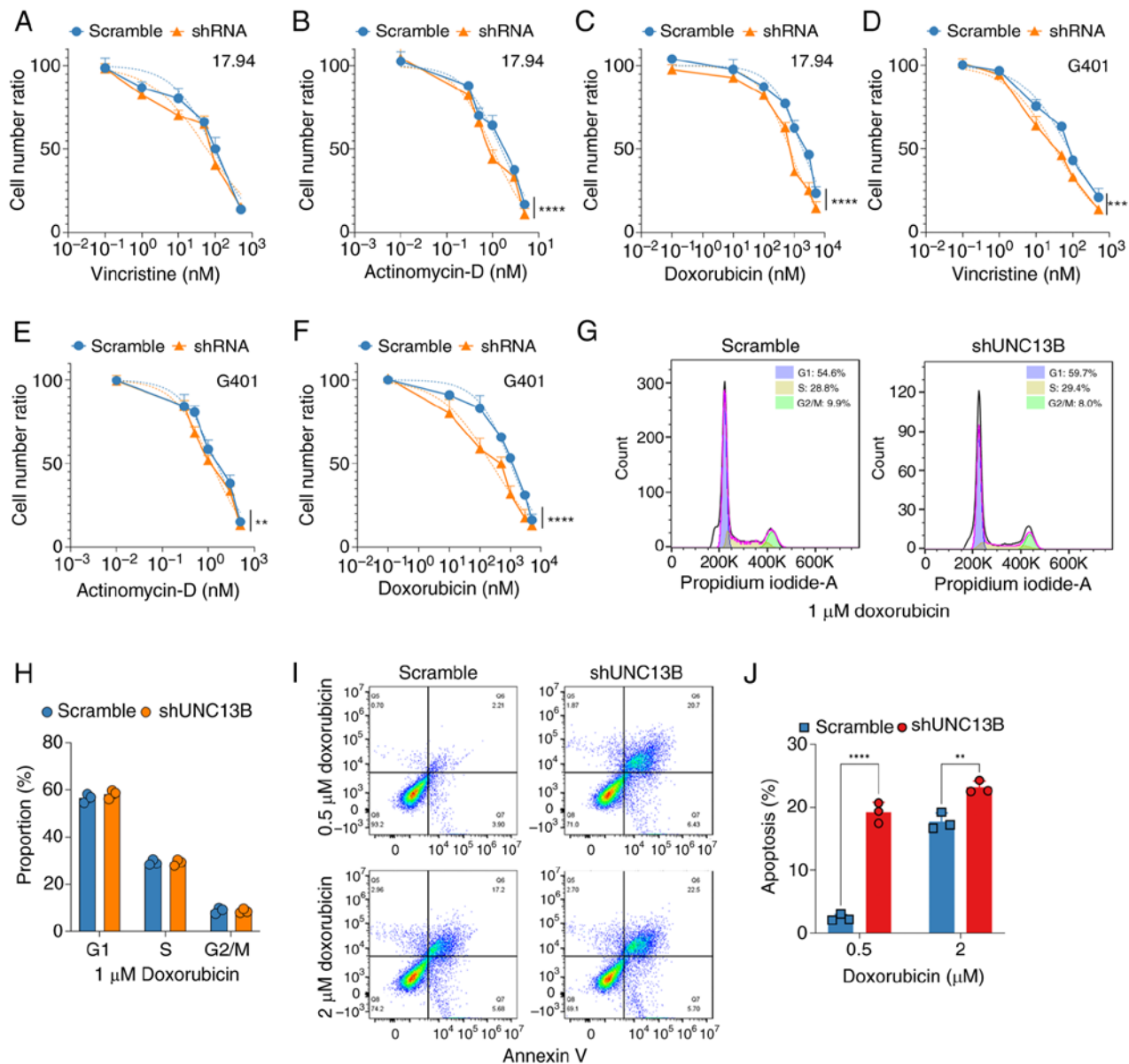


Figure 2. UNC13B influences Wilms' tumor sensitivity to chemotherapy drugs independent of the cell cycle. Evaluation of cell proliferation post-shRNA-mediated UNC13B knockdown after treatment with varying concentrations of (A) vincristine, (B) actinomycin-D and (C) doxorubicin for 48 h in 17.94 cells, and (D) vincristine, (E) actinomycin-D and (F) doxorubicin in the G401 cell line, assessed using Cell Counting Kit-8 assays. Changes in drug sensitivity were analyzed, with dashed lines representing fitted curves for half-maximal inhibitory concentration calculated using GraphPad software, and the cell number ratio indicating the relative number of viable cells compared between initial cell number and different time points. (G) Cell cycle analysis of 1 μ M doxorubicin treatment on control and shUNC13B knockdown cells, detected after 48 h post-drug treatment. (H) Quantification of the G1, S and G2 phases of the scramble and shUNC13B groups. (I) Typical pseudocolor scatter plots of the apoptosis analysis of UNC13B-knockdown 17.94 cells after 48 h treatment with 0.5 and 2 μ M doxorubicin, and (J) statistical results. ** $P < 0.01$; *** $P < 0.001$; **** $P < 0.0001$. UNC13B, unc-13 homolog B; sh, short hairpin.

indicating its potential involvement in vesicle-related functions. Furthermore, the lysosome status post-UNC13B knockdown was analyzed, revealing a significant decrease in lysosome level compared to the scramble group (Fig. 3B and C). This suggests that UNC13B may regulate lysosome formation through certain pathways.

UNC13B-induced lysosomal changes affect cell sensitivity to doxorubicin. The transfection efficiency of the 17.94 cell line was first evaluated using pCDNA3.1 as the expression vector. The results revealed a significant increase in the transcription level of UNC13B after transfection compared with the negative control, indicating that overexpression of UNC13B using

the transient transfection system was effective in the 17.94 cell line (Fig. 4A). To further assess the influence of UNC13B on lysosomes, the endogenous UNC13B was deleted, creating 17.94-delUNC13B. Subsequently, exogenous UNC13B was overexpressed in this cell line. The results demonstrated that the expression levels of LAMP1, a lysosome-associated protein, significantly increased in the 17.94 OE group compared to the 17.94 cell NC group, and decreased significantly in the 17.94 cell KO group compared to the 17.94 cell NC group (Fig. 4B and C). As UNC13B expression increased, the levels of LAMP1 expression also rose proportionally. Simultaneously, using Lyso-Tracker, a significant increase in lysosomal levels was observed in the 17.94 cell OE group compared to the 17.94

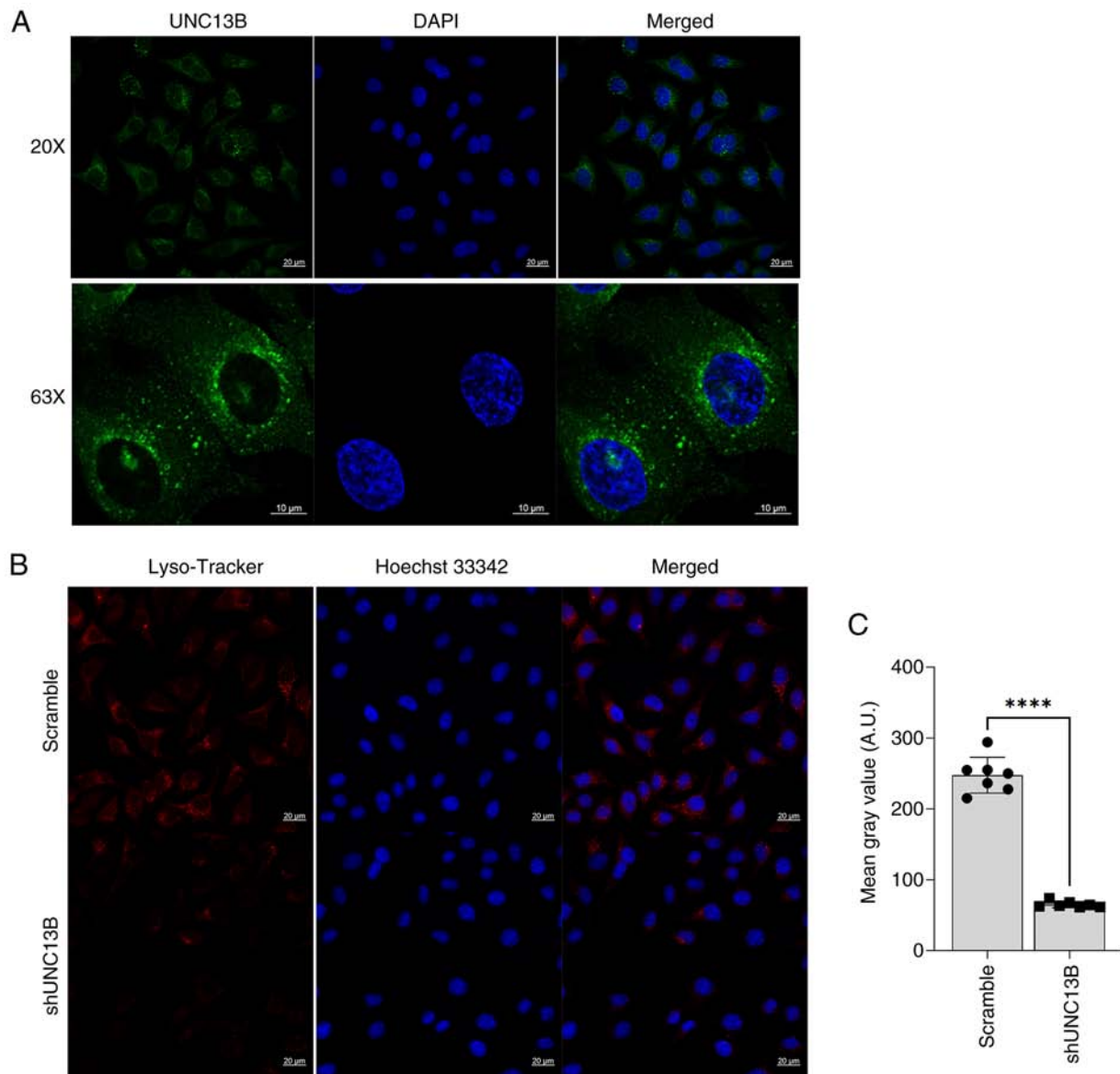


Figure 3. UNC13B localizes within vesicles and participates in regulating lysosome formation. (A) Indirect immunofluorescence detecting endogenous UNC13B expression in 17.94 cells and revealing UNC13B localization within cellular vesicles. Green fluorescence represents UNC13B and blue fluorescence represents the cell nucleus. (B) Staining of 17.94 cells with Lyso-Tracker. Cells were cultured in confocal culture dishes. The Mean Gray Value of red fluorescence was calculated in 7 different random fields using ImageJ software. Objective, 20X. (C) Mean Gray Value, calculated by measuring the grayscale values in indicated fluorescence channel regions of interest. ****P<0.0001. UNC13B, unc-13 homolog B; sh, short hairpin.

cell NC group, while a significant decrease was observed in the 17.94 cell KO group compared to the 17.94 cell NC group (Fig. 4D and E). These findings collectively indicate a clear positive association between lysosomal levels and UNC13B expression. The significant results compared the doxorubicin sensitivity between the 17.94 cell KO group and the 17.94 cell NC group, showing significantly increased sensitivity in the KO strain (1782 ± 101.3 vs. 702.9 ± 50.49 nM; Fig. 4F). Conversely, following UNC13B overexpression, there was a significant but minimal reduction in 17.94 sensitivity to doxorubicin compared to the 17.94 cell NC group (1782 ± 101.3 vs. 1928 ± 84.38 nM).

Discussion

Doxorubicin, also known as Adriamycin, is an anthracycline antibiotic derived from *Streptomyces peucetius*, exerting its

effect through several molecular mechanisms that induce cell death or growth arrest, including the inhibition of topoisomerase II, DNA intercalation and free radical production (25). Resistance of tumor cells to doxorubicin poses a significant challenge in its clinical use. Moreover, clinical studies have revealed late effects associated with doxorubicin, particularly cardiac system effects such as arrhythmias (26,27). Therefore, reducing drug dosage and lowering the doxorubicin's IC_{50} has become a critical need in clinical application. Mechanisms influencing doxorubicin drug sensitivity and resistance primarily involve epithelial-to-mesenchymal transition (28,29), alterations in topoisomerase II activity (30) and excessive activation of the ERK1/2 pathway (31). In addition to molecular changes, cells develop resistance by enhancing their detoxification capabilities, including reported overexpression of glutathione S-transferase (32). Notably, one key factor

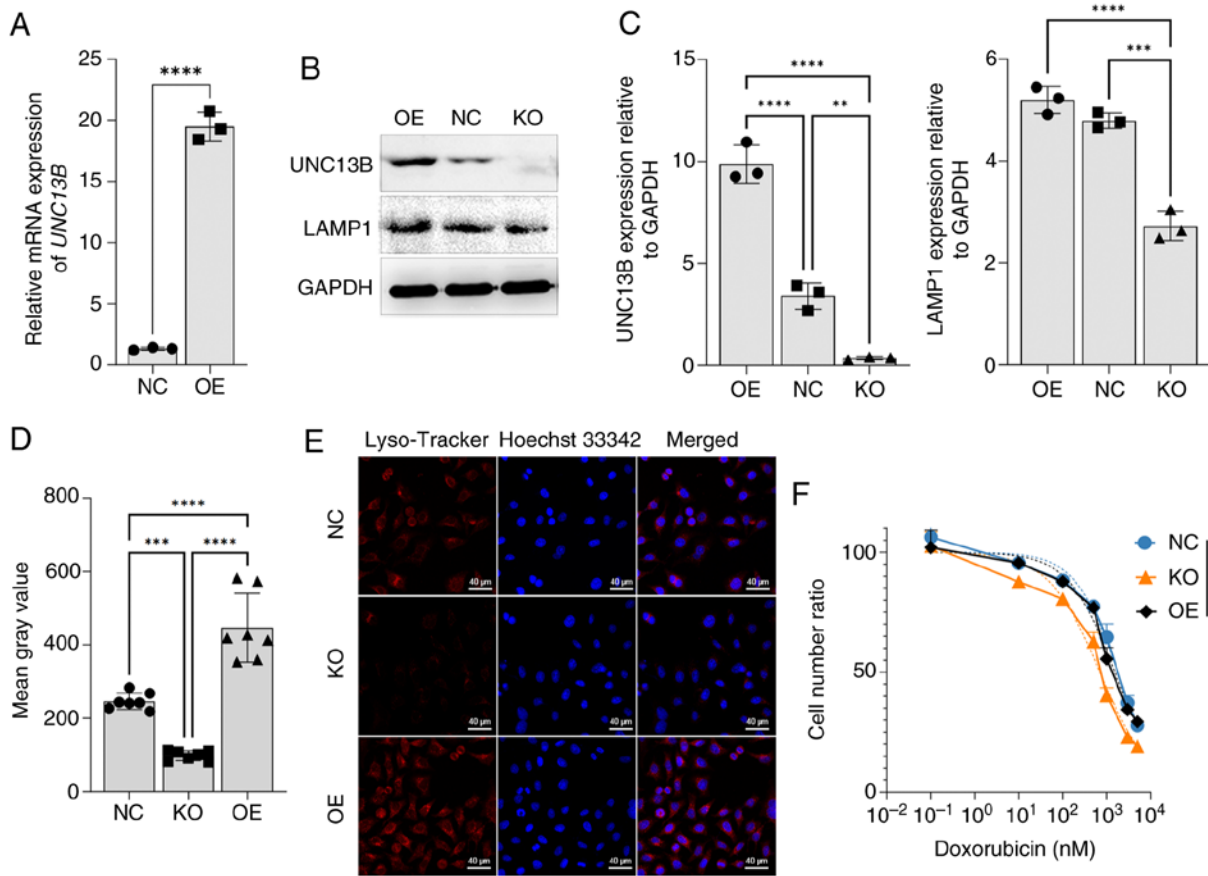


Figure 4. UNC13B modulates cell drug sensitivity by affecting lysosome formation. (A) 17.94 cell line was transiently transfected with the UNC13B-pCDNA3.1 overexpression vector using Lipofectamine 3,000. Reverse transcription-quantitative PCR validation was performed 24 h post-transfection. NC was the transfection with an empty pcDNA3.1 vector; $n=3$. (B) UNC13B and LAMP1 expression levels in 17.94 NC cells, UNC13B 17.94 OE cells and UNC13B 17.94 KO cells, using GAPDH as a reference, and (C) the associated semi-quantitative results. (D) Analysis of Mean Gray Value of Lyso-Tracker in 6 random fields of 17.94 NC, UNC13B 17.94 OE cells and UNC13B 17.94 KO cells, and (E) representative images of 17.94 NC cells, UNC13B 17.94 OE cells and UNC13B 17.94 KO cells. Lyso-Tracker indicated lysosomes, as the dye is highly selective for acidic environments, with an excitation wavelength of 577 nm and an emission wavelength of 590 nm. (F) Assessment of doxorubicin sensitivity changes in 17.94 NC, UNC13B 17.94 OE cells and UNC13B 17.94 KO cells; $n=3$. The cell number ratio indicates the relative number of viable cells compared between initial cell number and different time points. * $P<0.05$; ** $P<0.01$; *** $P<0.001$; **** $P<0.0001$. UNC13B, unc-13 homolog B; NC, negative control; OE, over-expressed; KO, knock-out; LAMP1, lysosomal-associated membrane protein 1.

in doxorubicin resistance is lysosomes (22). Research has reported doxorubicin accumulation in the lysosomes of resistant strains (33,34). In lymphoma cell lines, doxorubicin has been reported to be sequestered within lysosomes (22). In the present study, post-UNC13B knockdown, there was a decrease in the IC_{50} of doxorubicin in the Wilms' tumor 17.94 cell line, from 1882 ± 124.3 to 697.2 ± 46.29 nM (Fig. 2C), suggesting the involvement of UNC13B in the sensitivity of the tumor to doxorubicin. Furthermore, the results of the present study indicated that as lysosome quantity decreases in Wilms' tumor, 17.94 cells exhibited increased sensitivity to doxorubicin (Fig. 4D-F). After UNC13B knockdown, varying degrees of sensitivity changes to the other two drugs, vincristine and actinomycin-D, were also observed in 17.94 cells. However, these changes were not significant for vincristine ($P=0.0726$; Fig. 2A) or were significant but minor for actinomycin-D (1.544 ± 0.09 vs 1.005 ± 0.07 nM; $P<0.0001$; IC_{50} reduced by 50%; Fig. 2B). Therefore, further exploration of the mechanisms of sensitivity changes to vincristine and actinomycin-D in 17.94 cells after UNC13B knockdown was not pursued in the current study.

Lysosomes, a type of intracellular vesicle, are crucial for maintaining cellular homeostasis, digestion and breakdown

of aging cellular components and ingested nutrients (35,36). They also participate in cellular signaling regulation (37,38) and programmed cell death (39). Given the multifaceted functions of lysosomes, it is plausible that they serve a role in regulating cellular sensitivity to drugs. Extensive research has reported lysosome involvement in cellular drug sensitivity and resistance. Drugs captured by lysosomes via cationic chelation or sequestration led to drug isolation within the lysosomal acidic compartment, thereby isolating the drug's action on its target (40,41). Several chemotherapy drugs, including sunitinib (42), doxorubicin (43), rotenone (22) and vincristine (44), exhibited lysosomal capture, contributing to cell resistance. Additionally, lysosomes regulate cellular resistance through lysosome-mediated exocytosis (45). Due to the broad and critical role lysosomes serve in cellular sensitivity and resistance to drugs, researchers have targeted lysosomes to develop new strategies against resistance. These include altering drug structures (46), inhibiting key enzymes involved in lysosomal acidification (47,48) and interfering with intravesicular acidity (49). Several lysosomal proteins, including ion channels (50) and PINK-1 (51), could serve as specific targets to impair lysosomal activity, thereby selectively altering the drug

resistance characteristics of cancer cells. Changes in lysosomal function have been reported in several types of tumors, such as colorectal cancer (52) and gliomas (53). In cancer, tumor cells promote proliferation, migration and potentially resistance to chemotherapy by altering the number of lysosomes, the protein levels and activity of lysosomal hydrolases (54). In addition to the role in drug resistance mentioned in the present study, lysosomes also participate in the regulation of programmed cell death in tumor cells (55). Moreover, lysosomes can promote angiogenesis by secreting tissue proteases through exocytosis, activating Matrix metalloproteinases (56). Therefore, a wide range of candidate antitumor drugs has been developed targeting lysosomal organelle membranes (57), several Cathepsins contained within lysosomes (58), lysosomal pH (59) and key cellular processes involving lysosomes such as autophagy (60).

Most drugs targeting lysosomes in cancer research are still in the laboratory or preclinical stages. Among lysosome-mediated drugs in clinical research, hydroxychloroquine (HCQ) is a clinically approved and widely studied lysosome-related inhibitor. HCQ can inhibit autophagic degradation by blocking lysosomal acidification (61). Vogl *et al* (62) demonstrated in a Phase I trial that combining bortezomib (a proteasome inhibitor) with HCQ improved the efficacy of proteasome inhibition in multiple myeloma. A total of 45% of the 25 patients treated with the combination of HCQ and bortezomib demonstrated stable disease as their best response (62). Furthermore, in a clinical trial combining HCQ with the histone deacetylase inhibitor vorinostat, 24/27 treated patients were considered fully evaluable for study assessments and toxicity, including one patient with renal cell carcinoma showing durable partial response and two patients with colorectal cancer showing long-term stable disease (63). However, in a clinical trial for patients with malignant gliomas, the overall survival of patients with malignant gliomas was not notably improved when HCQ was used in combination with low-dose continuous temozolomide at a dose below the maximum tolerated dose (600 mg/day) (64). Additionally, low-dose, short-term use of HCQ has few side effects (65); however, at higher doses and longer durations, certain serious side effects have been observed, such as retinal toxicity (66). Therefore, improving the efficacy of HCQ should also be a focus of future research. We hypothesize that, as a gene involved in lysosome regulation, UNC13B will synergize with HCQ to achieve better efficacy.

In the present study, a significant positive association between UNC13B and lysosome formation was demonstrated (Fig. 4B-E). UNC13B participates in regulating vesicle precursor formation within neurons, essential for neurotransmitter storage and release (67). UNC13B, in collaboration with other proteins such as SNAP receptor proteins, facilitates vesicle fusion with the cell membrane (68). These findings suggest that in tumor cells, UNC13B may serve a role in vesicle maturation and regulation. The specific role of UNC13B in lysosome-mediated drug resistance involves several potential mechanisms based on its function in vesicular transport and its interactions with cellular organelles. UNC13B may influence the trafficking and fusion of lysosomes with autophagosomes or other vesicles. If UNC13B enhances the efficiency of lysosome fusion with autophagosomes, this may lead to more effective

sequestration and degradation of drugs, thereby contributing to drug resistance. As autophagy serves a role in drug resistance by degrading damaged organelles and proteins that could be targeted by chemotherapeutic agents, lysosomes may serve a central role in cellular autophagy (69). Furthermore, UNC13B may be involved in regulating the fusion of autophagy-related vesicles, a mechanism that could contribute to drug resistance. A UNC13 family protein, UNC13D has been reported to regulate the autophagy process (70). UNC13B may also influence the autophagy process by regulating the transport and fusion of vesicles, especially during the fusion step between autophagosomes and lysosomes. The results of the current study demonstrated a clear positive association between UNC13B levels and lysosomal levels, but the specific interactions and biological significance of UNC13B with lysosomes still need to be validated and clarified through further experimental research.

The findings of the present study should be validated using more Wilms' tumor cell lines; to the best of our knowledge, however, the only commercially available Wilms' tumor cell line is 17.94. Previous cell lines such as SK-NEP-1 and G401, which have been widely used for investigating Wilms' tumor mechanisms, are actually Ewing sarcoma and rhabdoid tumor cell lines, respectively (19,20). The use of only one Wilms' tumor cell line is acknowledged as a limitation of the present study, and it is suggested that additional Wilms' tumor cell lines would be used in future experiments to validate the findings. Although we have demonstrated a positive association between UNC13B levels and lysosome formation, the specific signaling pathways through which UNC13B regulates lysosome formation remain to be elucidated. Additionally, it is necessary to verify whether the regulatory role of UNC13B on lysosome formation is universal. Further studies are needed to determine if UNC13B can positively regulate lysosome formation in other cell lines as well.

In conclusion, the results of the present study demonstrated elevated expression of UNC13B in the Wilms' tumor cell line, 17.94, whilst its expression in normal cells (HK-2) remained low. This indicates that UNC13B could serve as a specific regulatory target for combined therapy with doxorubicin. Additionally, the results preliminarily demonstrated increased sensitivity to doxorubicin in 17.94 cells when UNC13B was inhibited. Furthermore, considering previous reports on lysosome-mediated resistance with drugs such as vincristine and rotenone, UNC13B holds promise as a target for combined therapy with such drugs. Lysosomes have become increasingly significant due to their role in cancer progression and resistance. However, lysosomal activity is crucial for almost all types of cells, hence, targeting them is generally not a cancer-specific strategy and may lead to severe adverse effects. Cancer-specific or cancer-enriched targets in this regard are still uncommon. The results of the present study suggest that UNC13B is likely an enriched target involved in lysosomal regulation in Wilms' tumor, providing a new intervention target for optimizing chemotherapy approaches in Wilms' tumor and other cancer types with high UNC13B expression.

Acknowledgements

Not applicable.

Funding

The present study was supported by the National Key R&D Program of China (grant no. 2022YFC2703500) and the Natural Science Foundation of Guangdong Province (grant no. 2019A1515110703).

Availability of data and materials

The data generated in the present study may be requested from the corresponding author.

Authors' contributions

JZ and XW contributed to the study conception and design. Material preparation, data collection and analysis were performed by XC, YB and GS. XC and XW confirm the authenticity of all the raw data. The first draft of the manuscript was written by XC and XW. All authors commented on previous versions of the manuscript. All the authors have read and approved the final manuscript.

Ethics approval and consent to participate

Not applicable.

Patient consent for publication

Not applicable.

Competing interests

The authors declare that they have no competing interests.

References

- Pastore G, Znaor A, Spreafico F, Graf N, Pritchard-Jones K and Steliarova-Foucher E: Malignant renal tumours incidence and survival in European children (1978-1997): Report from the automated childhood cancer information system project. *Eur J Cancer* 42: 2103-2114, 2006.
- Spreafico F, Fernandez CV, Brok J, Nakata K, Vujanic G, Geller JI, Gessler M, Maschietto M, Behjati S, Polanco A, *et al*: Wilms tumour. *Nat Rev Dis Primers* 7: 75, 2021.
- Dome JS, Graf N, Geller JI, Fernandez CV, Mullen EA, Spreafico F, Van den Heuvel-Eibrink M and Pritchard-Jones K: Advances in wilms tumor treatment and biology: Progress through international collaboration. *J Clin Oncol* 33: 2999-3007, 2015.
- Termuhlen AM, Tersak JM, Liu Q, Yasui Y, Stovall M, Weathers R, Deutsch M, Sklar CA, Oeffinger KC, Armstrong G, *et al*: Twenty-five year follow-up of childhood Wilms tumor: A report from the childhood cancer survivor study. *Pediatr Blood Cancer* 57: 1210-1216, 2011.
- Dome JS, Fernandez CV, Mullen EA, Kalapurakal JA, Geller JI, Huff V, Gratijs EJ, Dix DB, Ehrlich PF, Khanna G, *et al*: Children's oncology group's 2013 blueprint for research: Renal tumors. *Pediatr Blood Cancer* 60: 994-1000, 2013.
- Vujanic GM, Gessler M, Ooms A, Collini P, Coulomb-L'Hermine A, D'Hooghe E, de Krijger RR, Perotti D, Pritchard-Jones K, Vokuhl C, *et al*: The UMBRELLA SIOP-RTSG 2016 Wilms tumour pathology and molecular biology protocol. *Nat Rev Urol* 15: 693-701, 2018.
- Pritchard-Jones K, Bergeron C, de Camargo B, van den Heuvel-Eibrink MM, Acha T, Godzinski J, Oldenburger F, Boccon-Gibod L, Leuschner I, Vujanic G, *et al*: Omission of doxorubicin from the treatment of stage II-III, intermediate-risk Wilms' tumour (SIOP WT 2001): An open-label, non-inferiority, randomised controlled trial. *Lancet* 386: 1156-1164, 2015.
- Israels T, Moreira C, Scanlan T, Molyneux L, Kampondeni S, Hesselting P, Heij H, Borgstein E, Vujanic G, Pritchard-Jones K and Hadley L: SIOP PODC: Clinical guidelines for the management of children with Wilms tumour in a low income setting. *Pediatr Blood Cancer* 60: 5-11, 2013.
- van den Heuvel-Eibrink MM, Hol JA, Pritchard-Jones K, van Tinteren H, Furtwängler R, Verschuur AC, Vujanic GM, Leuschner I, Brok J, Rübe C, *et al*: Position paper: Rationale for the treatment of Wilms tumour in the UMBRELLA SIOP-RTSG 2016 protocol. *Nat Rev Urol* 14: 743-752, 2017.
- Kaste SC, Dome JS, Babyn PS, Graf NM, Grundy P, Godzinski J, Levitt GA and Jenkinson H: Wilms tumour: Prognostic factors, staging, therapy and late effects. *Pediatr Radiol* 38: 2-17, 2008.
- Wang XB, Yuan LH, Yan LP, Ye YB, Lu B and Xu X: UNC13B promote arsenic trioxide resistance in chronic lymphoid leukemia through mitochondria quality control. *Front Oncol* 12: 920999, 2022.
- Mansoori B, Mohammadi A, Davudian S, Shirjang S and Baradaran B: The different mechanisms of cancer drug resistance: A brief review. *Adv Pharm Bull* 7: 339-348, 2017.
- Pooryasin A, Maglione M, Schubert M, Matkovic-Rachid T, Hasheminasab SM, Pech U, Fiala A, Mielke T and Sigrist SJ: Unc13A and Unc13B contribute to the decoding of distinct sensory information in *Drosophila*. *Nat Commun* 12: 1932, 2021.
- Green TE, Scheffer IE, Berkovic SF and Hildebrand MS: UNC13B and focal epilepsy. *Brain* 145: e10-e12, 2022.
- Corrigendum to: UNC13B variants associated with partial epilepsy with favourable outcome. *Brain* 145: e5, 2022.
- Warr MR, Binnewies M, Flach J, Reynaud D, Garg T, Malhotra R, Debnath J and Passequé E: FOXO3A directs a protective autophagy program in haematopoietic stem cells. *Nature* 494: 323-327, 2013.
- Livak KJ and Schmittgen TD: Analysis of relative gene expression data using real-time quantitative PCR and the 2(-Delta Delta C(T)) method. *Methods* 25: 402-408, 2001.
- Brown KW, Charles A, Dallosso A, White G, Charlet J, Standen GR and Malik K: Characterization of 17.94, a novel anaplastic Wilms' tumor cell line. *Cancer Gene* 205: 319-326, 2012.
- Smith MA, Morton CL, Phelps D, Girtman K, Neale G and Houghton PJ: SK-NP-1 and Rh1 are Ewing family tumor lines. *Pediatr Blood Cancer* 50: 703-706, 2008.
- Garvin AJ, Re GG, Tarnowski BI, Hazen-Martin DJ and Sens DA: The G401 cell line, utilized for studies of chromosomal changes in Wilms' tumor, is derived from a rhabdoid tumor of the kidney. *Am J Pathol* 142: 375-380, 1993.
- Oostveen RM and Pritchard-Jones K: Pharmacotherapeutic management of wilms tumor: An update. *Paediatr Drugs* 21: 1-13, 2019.
- Hurwitz SJ, Terashima M, Mizunuma N and Slapak CA: Vesicular anthracycline accumulation in doxorubicin-selected U-937 cells: Participation of lysosomes. *Blood* 89: 3745-3754, 1997.
- Wang J, Qiao JD, Liu XR, Liu DT, Chen YH, Wu Y, Sun Y, Yu J, Ren RN, Mei Z, *et al*: UNC13B variants associated with partial epilepsy with favourable outcome. *Brain* 144: 3050-3060, 2021.
- Bohme MA, Beis C, Reddy-Alla S, Reynolds E, Mampell MM, Grasskamp AT, Lützkendorf J, Bergeron DD, Driller JH, Babikir H, *et al*: Active zone scaffolds differentially accumulate Unc13 isoforms to tune Ca(2+) channel-vesicle coupling. *Nat Neurosci* 19: 1311-1320, 2016.
- Meredith AM and Dass CR: Increasing role of the cancer chemotherapeutic doxorubicin in cellular metabolism. *J Pharm Pharmacol* 68: 729-741, 2016.
- Murtagh G, Lyons T, O'Connell E, Ballot J, Geraghty L, Fennelly D, Gullo G, Ledwidge M, Crown J, Gallagher J, *et al*: Late cardiac effects of chemotherapy in breast cancer survivors treated with adjuvant doxorubicin: 10-year follow-up. *Breast Cancer Res Treat* 156: 501-506, 2016.
- Kilickap S, Barista I, Akgul E, Aytemir K, Aksoy S and Tekuzman G: Early and late arrhythmogenic effects of doxorubicin. *South Med J* 100: 262-265, 2007.
- Saxena M, Stephens MA, Pathak H and Rangarajan A: Transcription factors that mediate epithelial-mesenchymal transition lead to multidrug resistance by upregulating ABC transporters. *Cell Death Dis* 2: e179, 2011.
- Xu T, Zhang J, Chen W, Pan S, Zhi X, Wen L, Zhou Y, Chen BW, Qiu J, Zhang Y, *et al*: ARK5 promotes doxorubicin resistance in hepatocellular carcinoma via epithelial-mesenchymal transition. *Cancer Lett* 377: 140-148, 2016.

30. Withoff S, De Jong S, De Vries EG and Mulder NH: Human DNA topoisomerase II: Biochemistry and role in chemotherapy resistance (review). *Anticancer Res* 16: 1867-1880, 1996.
31. Shukla A, Hillegass JM, MacPherson MB, Beuschel SL, Vacek PM, Pass HI, Carbone M, Testa JR and Mossman BT: Blocking of ERK1 and ERK2 sensitizes human mesothelioma cells to doxorubicin. *Mol Cancer* 9: 314, 2010.
32. Singh SV, Nair S, Ahmad H, Awasthi YC and Krishan A: Glutathione S-transferases and glutathione peroxidases in doxorubicin-resistant murine leukemic P388 cells. *Biochem Pharmacol* 38: 3505-3510, 1989.
33. Guo B, Tam A, Santi SA and Parissenti AM: Role of autophagy and lysosomal drug sequestration in acquired resistance to doxorubicin in MCF-7 cells. *BMC Cancer* 16: 762, 2016.
34. Seebacher NA, Richardson DR and Jansson PJ: A mechanism for overcoming P-glycoprotein-mediated drug resistance: Novel combination therapy that releases stored doxorubicin from lysosomes via lysosomal permeabilization using Dp44mT or DpC. *Cell Death Dis* 7: e2510, 2016.
35. Lamming DW and Bar-Peled L: Lysosome: The metabolic signaling hub. *Traffic* 20: 27-38, 2019.
36. Mahapatra KK, Mishra SR, Behera BP, Patil S, Gewirtz DA and Bhutia SK: The lysosome as an imperative regulator of autophagy and cell death. *Cell Mol Life Sci* 78: 7435-7449, 2021.
37. Yang C and Wang X: Lysosome biogenesis: Regulation and functions. *J Cell Biol* 220: e202102001, 2021.
38. Perera RM and Zoncu R: The lysosome as a regulatory hub. *Annu Rev Cell Dev Biol* 32: 223-253, 2016.
39. Patra S, Patil S, Klionsky DJ and Bhutia SK: Lysosome signaling in cell survival and programmed cell death for cellular homeostasis. *J Cell Physiol* 238: 287-305, 2023.
40. Adar Y, Stark M, Bram EE, Nowak-Sliwinska P, van den Bergh H, Szewczyk G, Sarna T, Skladanowski A, Griffioen AW and Assaraf YG: Imidazoacridinone-dependent lysosomal photodestruction: A pharmacological Trojan horse approach to eradicate multidrug-resistant cancers. *Cell Death Disease* 3: e293, 2012.
41. Kaufmann AM and Krise JP: Lysosomal sequestration of amine-containing drugs: Analysis and therapeutic implications. *J Pharma Sci* 96: 729-746, 2007.
42. Gotink KJ, Broxterman HJ, Labots M, de Haas RR, Dekker H, Honeywell RJ, Rudek MA, Beerepoot LV, Musters RJ, Jansen G, *et al*: Lysosomal sequestration of sunitinib: A novel mechanism of drug resistance. *Clin Cancer Res* 17: 7337-7346, 2011.
43. Herlevsen M, Oxford G, Owens CR, Conaway M and Theodorescu D: Depletion of major vault protein increases doxorubicin sensitivity and nuclear accumulation and disrupts its sequestration in lysosomes. *Mol Cancer Ther* 6: 1804-1813, 2007.
44. Groth-Pedersen L, Ostenfeld MS, Hoyer-Hansen M, Nylandsted J and Jäättelä M: Vincristine induces dramatic lysosomal changes and sensitizes cancer cells to lysosome-destabilizing siramesine. *Cancer Res* 67: 2217-2225, 2007.
45. Yanes RE, Tarn D, Hwang AA, Ferris DP, Sherman SP, Thomas CR, Lu J, Pyle AD, Zink JI and Tamanoi F: Involvement of lysosomal exocytosis in the excretion of mesoporous silica nanoparticles and enhancement of the drug delivery effect by exocytosis inhibition. *Small* 9: 697-704, 2013.
46. Duvvuri M, Konkari S, Funk RS, Krise JM and Krise JP: A chemical strategy to manipulate the intracellular localization of drugs in resistant cancer cells. *Biochemistry* 44: 15743-15749, 2005.
47. Ouar Z, Bens M, Vignes C, Paulais M, Pringel C, Fleury J, Cluzeaud F, Lacave R and Vandewalle A: Inhibitors of vacuolar H⁺-ATPase impair the preferential accumulation of daunomycin in lysosomes and reverse the resistance to anthracyclines in drug-resistant renal epithelial cells. *Biochem J* 370: 185-193, 2003.
48. Hrabeta J, Groh T, Khalil MA, Poljakova J, Adam V, Kizek R, Uhlik J, Doktorova H, Cerna T, Frei E, *et al*: Vacuolar-ATPase-mediated intracellular sequestration of ellipticine contributes to drug resistance in neuroblastoma cells. *Int J Oncol* 47: 971-980, 2015.
49. Kazmi F, Hensley T, Pope C, Funk RS, Loewen GJ, Buckley DB and Parkinson A: Lysosomal sequestration (trapping) of lipophilic amine (cationic amphiphilic) drugs in immortalized human hepatocytes (Fa2N-4 cells). *Drug Metab Dispos* 41: 897-905, 2013.
50. Geisslinger F, Muller M, Vollmar AM and Bartel K: Targeting lysosomes in cancer as promising strategy to overcome chemoresistance-a mini review. *Front Oncol* 10: 1156, 2020.
51. Dykstra KM, Fay HRS, Massey AC, Yang N, Johnson M, Portwood S, Guzman ML and Wang ES: Inhibiting autophagy targets human leukemic stem cells and hypoxic AML blasts by disrupting mitochondrial homeostasis. *Blood Adv* 5: 2087-2100, 2021.
52. Abdulla MH, Valli-Mohammed MA, Al-Khayal K, Al Shkiah A, Zubaidi A, Ahmad R, Al-Saleh K, Al-Obeid O and McKerrrow J: Cathepsin B expression in colorectal cancer in a Middle East population: Potential value as a tumor biomarker for late disease stages. *Oncol Rep* 37: 3175-3180, 2017.
53. Fukuda ME, Iwadate Y, Machida T, Hiwasa T, Nimura Y, Nagai Y, Takiguchi M, Tanzawa H, Yamaura A and Seki N: Cathepsin D is a potential serum marker for poor prognosis in glioma patients. *Cancer Res* 65: 5190-5194, 2005.
54. Davidson SM and Heiden MG: Critical functions of the lysosome in cancer biology. *Ann Rev Pharmacol Toxicol* 57: 481-507, 2017.
55. Iulianna T, Kuldeep N and Eric F: The Achilles' heel of cancer: Targeting tumors via lysosome-induced immunogenic cell death. *Cell Death Dis* 13: 509, 2022.
56. Kallunki T, Olsen OD and Jäättelä M: Cancer-associated lysosomal changes: Friends or foes? *Oncogene* 32: 1995-2004, 2013.
57. Boya P and Kroemer G: Lysosomal membrane permeabilization in cell death. *Oncogene* 27: 6434-6451, 2008.
58. Groth-Pedersen L and Jäättelä M: Combating apoptosis and multidrug resistant cancers by targeting lysosomes. *Cancer Lett* 332: 265-274, 2013.
59. Manic G, Obrist F, Kroemer G, Vitale I and Galluzzi L: Chloroquine and hydroxychloroquine for cancer therapy. *Mol Cell Oncol* 1: e29911, 2014.
60. Dufour M, Dormond-Meuwly A, Demartines N and Dormond O: Targeting the mammalian target of rapamycin (mTOR) in cancer therapy: Lessons from past and future perspectives. *Cancers (Basel)* 3: 2478-2500, 2011.
61. Pellegrini P, Strambi A, Zipoli C, Hägg-Olofsson M, Buoncervello M, Linder S and De Milito A: Acidic extracellular pH neutralizes the autophagy-inhibiting activity of chloroquine: Implications for cancer therapies. *Autophagy* 10: 562-571, 2014.
62. Vogl DT, Stadtmayer EA, Tan KS, Heitjan DF, Davis LE, Pontiggia L, Rangwala R, Piao S, Chang YC, Scott EC, *et al*: Combined autophagy and proteasome inhibition: A phase I trial of hydroxychloroquine and bortezomib in patients with relapsed/refractory myeloma. *Autophagy* 10: 1380-1390, 2014.
63. Mahalingam D, Mita M, Sarantopoulos J, Wood L, Amaravadi RK, Davis LE, Mita AC, Curiel TJ, Espitia CM, Nawrocki ST, *et al*: Combined autophagy and HDAC inhibition: A phase I safety, tolerability, pharmacokinetic, and pharmacodynamic analysis of hydroxychloroquine in combination with the HDAC inhibitor vorinostat in patients with advanced solid tumors. *Autophagy* 10: 1403-1414, 2014.
64. Rosenfeld MR, Ye X, Supko JG, Desideri S, Grossman SA, Brem S, Mikkelsen T, Wang D, Chang YC, Hu J, *et al*: A phase I/II trial of hydroxychloroquine in conjunction with radiation therapy and concurrent and adjuvant temozolomide in patients with newly diagnosed glioblastoma multiforme. *Autophagy* 10: 1359-1368, 2014.
65. Amaravadi RK, Lippincott-Schwartz J, Yin XM, Weiss WA, Takebe N, Timmer W, DiPaola RS, Lotze MT and White E: Principles and current strategies for targeting autophagy for cancer treatment. *Clin Cancer Res* 17: 654-666, 2011.
66. Rangwala R, Leone R, Chang YC, Fecher LA, Schuchter LM, Kramer A, Tan KS, Heitjan DF, Rodgers G, Gallagher M, *et al*: Phase I trial of hydroxychloroquine with dose-intense temozolomide in patients with advanced solid tumors and melanoma. *Autophagy* 10: 1369-1379, 2014.
67. Rossner S, Fuchsbrunner K, Lange-Dohna C, Hartlage-Rübsamen M, Bigl V, Betz A, Reim K and Brose N: Munc13-1-mediated vesicle priming contributes to secretory amyloid precursor protein processing. *J Biol Chem* 279: 27841-27844, 2004.
68. Dittman JS: Unc13: A multifunctional synaptic marvel. *Curr Opin Neurobiol* 57: 17-25, 2019.
69. Yamamoto H, Zhang S and Mizushima N: Autophagy genes in biology and disease. *Nat Rev Gene* 24: 382-400, 2023.
70. Zhang J, He J, Johnson JL, Napolitano G, Ramadass M, Rahman F and Catz SD: Cross-regulation of defective endolysosome trafficking and enhanced autophagy through TFEB in UNC13D deficiency. *Autophagy* 15: 1738-1756, 2019.

